

## A CHANDRA OBSERVATION OF ABELL 13: INVESTIGATING THE ORIGIN OF THE RADIO RELIC

ADRIENNE M. JUETT<sup>1</sup>, CRAIG L. SARAZIN<sup>1</sup>, TRACY E. CLARKE<sup>2</sup>, HEINZ ANDERNACH<sup>3</sup>, MATTHIAS EHLE<sup>4</sup>, YUTAKA FUJITA<sup>5</sup>,  
JOSHUA C. KEMPNER<sup>6</sup>, ALAN L. ROY<sup>7</sup>, LAWRENCE RUDNICK<sup>8</sup>, AND O. BRUCE SLEE<sup>9</sup>

*Accepted for publication in the Astrophysical Journal*

### ABSTRACT

We present results from the *Chandra* X-ray observation of Abell 13, a galaxy cluster that contains an unusual noncentral radio source, also known as a radio relic. This is the first pointed X-ray observation of Abell 13, providing a more sensitive study of the properties of the X-ray gas. The X-ray emission from Abell 13 is extended to the northwest of the X-ray peak and shows substructure indicative of a recent merger event. The cluster X-ray emission is centered on the bright galaxy H of Slee et al. (2001). We find no evidence for a cooling flow in the cluster. A knot of excess X-ray emission is coincident with the other bright elliptical galaxy F. This knot of emission has properties similar to the enhanced emission associated with the large galaxies in the Coma cluster.

With these *Chandra* data we are able to compare the properties of the hot X-ray gas with those of the radio relic from VLA data, to study the interaction of the X-ray gas with the radio emitting electrons. Our results suggest that the radio relic is associated with cooler gas in the cluster. We suggest two explanations for the coincidence of the cooler gas and radio source. First, the gas may have been uplifted by the radio relic from the cluster core. Alternatively, the relic and cool gas may have been displaced from the central galaxy during the cluster merger event.

*Subject headings:* galaxies: clusters: general — galaxies: clusters: individual (A13) — X-rays: galaxies: clusters — radio continuum: galaxies — intergalactic medium

### 1. INTRODUCTION

The high spatial resolution of the *Chandra X-ray Observatory* allows us to study the intracluster medium (ICM) in clusters of galaxies in unprecedented detail. One interesting result is the interplay between the X-ray emitting gas and non-thermal radio emission. Observations of several galaxy clusters have found X-ray cavities in the ICM coincident with bright radio emission (e.g., Perseus (A 426); Böhringer et al. 1993; Fabian et al. 2000). The central radio sources produce the bubbles of non-thermal plasma responsible for the radio emission. These bubbles then rise, possibly by buoyancy, displacing the X-ray emitting gas and causing cavities in the latter.

A number of galaxy clusters contain large-scale diffuse radio sources not associated with active galactic nuclei. These sources are classified into two groups: radio halos which are centrally located, and radio relics. Radio relics

are extended diffuse radio sources often located at the periphery of clusters of galaxies. Giovannini & Feretti (2004) present a classification scheme for radio relics based on their observational properties (but see also Kempner et al. 2004). Radio relics typically have steep radio spectra ( $\alpha > 1$  assuming  $S_\nu \propto \nu^{-\alpha}$ ) and are linearly polarized (Giovannini & Feretti 2004). The X-ray surface brightness around most radio relics is low, making it difficult to study the relationship between the X-ray gas and radio emission.

Many radio relics, including some of the best known and studied (e.g., the Coma cluster relic 1253+275 and Abell 3667; Giovannini et al. 1991; Röttgering et al. 1997), are located far from the cluster center, on the order of Mpcs. However, there exists a subclass of radio relics which are located significantly closer to the cluster center,  $\sim 50$  to 350 kpc. Giovannini & Feretti (2004) classify these as relic sources near the first ranked galaxy. These radio sources share many of the same properties of classical radio relics including steep spectra, filamentary structure, and polarization (Slee et al. 2001). Abell 133 is one of the class of radio relics near the first ranked galaxy. A *Chandra* observation revealed a tongue-like feature in the X-ray emission comprised of cool gas ( $kT \approx 1.3$  keV) which extended from the cD galaxy to the radio relic (Fujita et al. 2002). A number of possible origins for the tongue were explored including the suggestion that the cool gas in the tongue was uplifted from the cluster core by the buoyantly rising radio relic. A followup observation with *XMM-Newton* is consistent with the uplifted bubble scenario (Fujita et al. 2004). However the detection of a cold front southeast of the cluster core and a weak shock in the core suggests that an unequal mass merger is responsible for the tongue feature. In either model, the radio plasma appears to have originated from the active galactic nucleus

<sup>1</sup> Department of Astronomy, University of Virginia, P.O. Box 400325, Charlottesville, VA 22904-4325, USA; ajuett@virginia.edu, sarazin@virginia.edu

<sup>2</sup> Naval Research Laboratory, 4555 Overlook Ave. SW, Code 7213, Washington, DC 20375, USA; Interferometrics Inc., 13454 Sunrise Valley Drive, Suite 240, Herndon, VA 20171, USA

<sup>3</sup> Departamento de Astronomía, Universidad de Guanajuato, AP 144, Guanajuato CP 36000, Mexico

<sup>4</sup> XMM-Newton Science Operations Centre, European Space Agency, Villafranca del Castillo, P.O. Box 50727, 28080 Madrid, Spain

<sup>5</sup> Department of Earth and Space Science, Graduate School of Science, Osaka University, Toyonaka, Osaka 560-0043, Japan

<sup>6</sup> Department of Physics and Astronomy, Bowdoin College, 8800 College Station, Brunswick, ME 04011, USA

<sup>7</sup> Max-Planck-Institut für Radioastronomie, Auf dem Hügel 69, D-53121 Bonn, Germany

<sup>8</sup> University of Minnesota, 116 Church St SE, Minneapolis, MN 55455, USA

<sup>9</sup> Australia Telescope National Facility, P.O. Box 76, Epping, NSW 2121, Australia

TABLE 1  
 PROPERTIES OF DETECTED POINT SOURCES IN ABELL 13 FIELD

Name	R.A. <sup>a</sup>	Dec. <sup>a</sup>	Count Rate ( $10^{-3} \text{ s}^{-1}$ )
CXOU J001316.6–193201	00:13:16.67	–19:32:01.2	6.3±0.4
CXOU J001319.0–193018	00:13:19.09	–19:30:18.5	0.43±0.12
CXOU J001320.0–192748	00:13:20.06	–19:27:48.6	2.1±0.2
CXOU J001321.9–192750	00:13:21.98	–19:27:50.7	2.4±0.2
CXOU J001326.0–193111	00:13:26.02	–19:31:11.4	3.9±0.3
CXOU J001335.7–192805	00:13:35.74	–19:28:05.5	0.61±0.14
CXOU J001339.9–192935	00:13:39.94	–19:29:35.8	4.2±0.3
CXOU J001341.1–192809	00:13:41.15	–19:28:09.5	1.8±0.2
CXOU J001342.5–193209	00:13:42.58	–19:32:09.0	0.54±0.13
CXOU J001344.6–192914	00:13:44.60	–19:29:14.1	0.38±0.11
CXOU J001344.7–193051	00:13:44.70	–19:30:51.0	4.6±0.3

<sup>a</sup> Units of right ascension are hours, minutes, and seconds, and units of declination are degrees, arcminutes, and arcseconds. The 90% uncertainty in absolute positional accuracy of *Chandra* is 0'6.

(AGN) in the central cD, rather than as a direct result of merger shock acceleration.

In this paper, we present X-ray data obtained with the *Chandra X-ray Observatory* for the cluster Abell 13, another unusual system with a radio relic near the first ranked galaxy. Abell 13 is an X-ray luminous ( $8 \times 10^{43} \text{ erg s}^{-1}$  in the 0.5–10 keV range) cluster at  $z = 0.0943$  (Mazure et al. 1996). The relic has an extremely steep ( $\alpha \approx 4$ ) radio spectrum, a linear polarization of  $\approx 12\%$  at 1425 MHz, and spans up to  $2'$  (Slee et al. 2001). No identification of a host galaxy associated with the relic was possible, although the two brightest cluster members are candidates. Interestingly, these two galaxies are separated by  $2621 \text{ km s}^{-1}$  in recession velocity (Quintana & Ramírez 1995). Similarly, from redshift data of the ESO Nearby Abell Clusters Survey (ENACS), Fadda et al. (1996) concluded that the radial velocity distribution of Abell 13 may also be interpreted as a bimodal one, with peaks at  $z = 0.0919$  (16 redshifts, vel.disp.  $361_{-35}^{+53} \text{ km s}^{-1}$ ) and 0.0972 (21 redshifts vel.disp.  $515_{-81}^{+104} \text{ km s}^{-1}$ ), or  $\langle cz \rangle = 27570$  and  $29160 \text{ km s}^{-1}$ . We assume  $H_0 = 70 \text{ km s}^{-1} \text{ Mpc}^{-1}$ ,  $\Omega_M = 0.3$ , and  $\Omega_\Lambda = 0.7$  unless otherwise mentioned. At the distance of Abell 13,  $1''$  corresponds to 1.75 kpc.

## 2. SPATIAL ANALYSIS

We observed Abell 13 on 2004 August 25 for 55 ks with *Chandra* using the Advanced CCD Imaging Spectrometer (ACIS; Garmire et al. 2003). The observation was performed so that both the cluster center and the radio relic were located on the back-illuminated S3 CCD. The ‘‘level 1’’ event file was processed using the CIAO v3.2 data analysis package<sup>10</sup> following the standard reduction procedure. We removed the afterglow correction and created a new observation specific bad pixel file. The level 1 event file was reprocessed to include the new bad pixel file and utilize the improved background event detection in VFAINT mode. We then filtered the data to remove hot pixels, bad columns, and events with grades 1, 3, 5, and 7. Data from the back-illuminated S1 CCD were used to determine time intervals with high background using the tool `lc_clean`. We filtered the event file on good times, yielding a final exposure time of 50.7 ks. Background data were extracted from the blank sky ob-

servations compiled by M. Markevitch<sup>11</sup>. Our analysis is restricted to data from the S3 CCD.

In Figure 1, we show both the raw *Chandra* X-ray image of the 0.3–10 keV energy range, and an adaptively smoothed image of the X-ray data produced with the CIAO tool `csmooth`. The smoothed image has a minimum signal-to-noise ratio of 3 per smoothing beam, and has been corrected for exposure and background. The X-ray emission from Abell 13 shows complex structure in the core region. A knot of X-ray emission is also clearly detected  $86''$  (150 kpc) to the northwest of the cluster’s X-ray peak, along with a more diffuse extension of the emission in the same direction.

We identify 11 point sources in our full band image (0.3–10.0 keV; see Table 1). This is consistent with the expected number of background sources from the *Chandra* Deep Fields (Brandt et al. 2001; Giacconi et al. 2001). No point source was found at the center of the X-ray emission. Since the cluster emission will reduce our point source detection sensitivity, we also searched for point sources in just the hard band (4.0–10.0 keV) data. In the hard X-ray band, the diffuse emission from the cluster is weaker while the emission from AGN is stronger than at softer bands. Therefore, any AGNs should be more easily detected. We found no point sources within  $0'5$  of the cluster center, defined to be the position of galaxy H, the brightest cluster galaxy.

In Figure 2, we show the optical Digital Sky Survey (DSS) image<sup>12</sup> of the cluster with the X-ray contours overlaid. The X-ray contours are based on the image in Figure 1 *right panel*. We have labeled the brightest galaxies following Slee et al. (2001). The X-ray emission is centered near the bright elliptical H (also 2MASX J00133853–1930007), the brightest cluster galaxy. The knot of emission to the NW is coincident with the elliptical galaxy F (also 2MASX J00133401–1929017), the second brightest cluster galaxy. The steepness of the X-ray gradient to the north and east is an artifact of the CCD edges.

We are also interested in comparing the X-ray data with the radio emission from Abell 13. Figure 3 shows the X-ray data in red and the radio data in green. We find no enhancement of the X-ray emission near the radio relic, which is different from what was seen for Abell

<sup>11</sup> See [http://cxc.harvard.edu/cal/Acis/Cal\\_prods/bkgnd/acisbg/](http://cxc.harvard.edu/cal/Acis/Cal_prods/bkgnd/acisbg/)

<sup>12</sup> Available at <http://archive.stsci.edu/dss/>

<sup>10</sup> <http://asc.harvard.edu/ciao/>

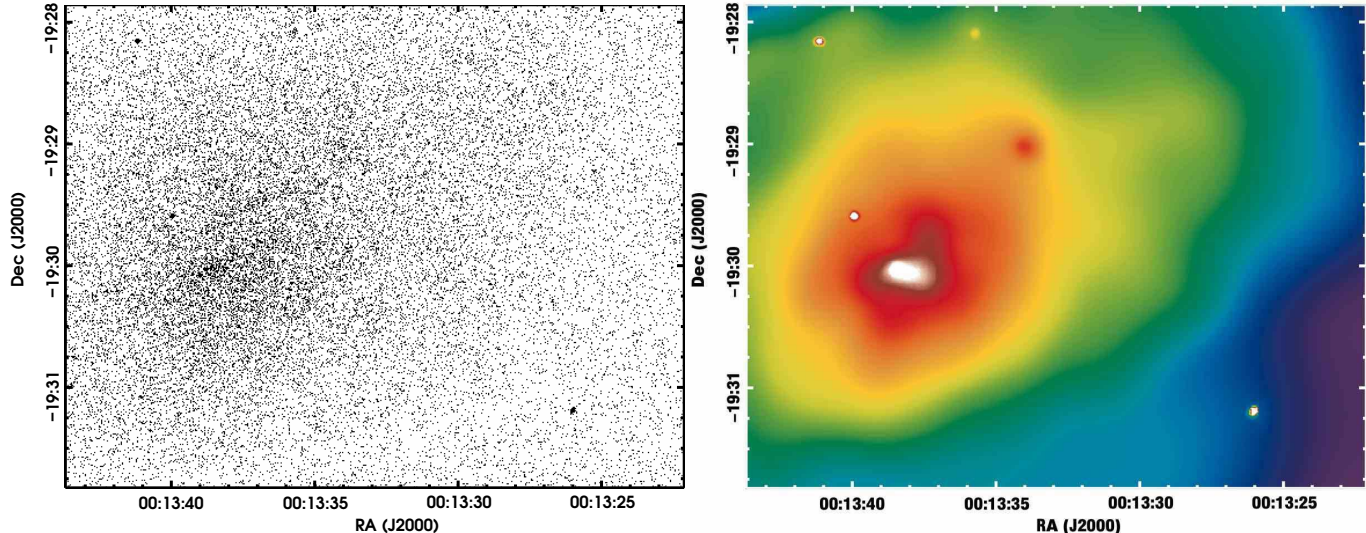


FIG. 1.— *Left Panel:* Raw *Chandra* X-ray image (0.3–10 keV) of the  $5' \times 4'$  region of Abell 13 encompassing the cluster center and radio relic positions. The image is uncorrected for exposure or background. North is up, and east is left. The image pixels are  $0''.492$ . *Right Panel:* Adaptively smoothed *Chandra* X-ray image of the same region, corrected for background, exposure, and vignetting. Notice the structure in the X-ray core as well as the knot of emission to the northwest of the core. In addition, the X-ray emission is extended to the northwest and west (towards the radio relic). The number of point sources is consistent with that expected from background sources.

133 (Fujita et al. 2002). Given the low surface brightness of the X-ray emission, it is difficult to determine if there is a deficit of X-ray emission at the position of the radio relic, commonly referred to as an X-ray cavity or radio bubble. The absolute astrometric accuracy of the radio and X-ray maps is roughly  $0''.5$  for each. The radio point source near the cluster center is not associated with galaxy H. Instead, it seems coincident with a barely resolved pair of galaxies in the DSS and Two Micron All Sky Survey (2MASS) images, listed in NED<sup>13</sup> as 2MASX J00133712–1930067. No velocity information is available for 2MASX J00133712–1930067, making association with the cluster uncertain.

To enhance the structures in the cluster core, we fitted the observed cluster emission with a smooth elliptical isophotal model, using the IRAF/STSDAS task `ellipse`. We allowed the ellipticity, position angle, and intensities of each isophote to vary while keeping the centroids fixed to the position of galaxy H. The model was then subtracted from the data after multiplication of the model counts by 0.5 to avoid over-subtraction. In Figure 4, we show the subtracted image of the cluster in the region around the radio relic with the radio contours overlaid. No excess emission is associated with the radio relic. The cluster emission is faint near the radio relic, and continues to weaken at projected cluster-centric distances greater than that of the relic in the same direction.

More interesting structure is seen in the cluster center. Figure 5 shows the same image as Figure 4 with a different color scale to enhance the variations in the inner region of the cluster. The knot of emission in the upper right is the second-brightest elliptical galaxy, F. The bright yellow knot of emission is coincident with galaxy H. There is a more diffuse bright extension of emission to the west of galaxy H. In addition, there is other structure in the cluster center perpendicular to the bright extension. Interestingly, the emission extension to the west of galaxy H seems to point in the same direction as one

might expect the radio relic to extend if it were projected back to galaxy H.

### 2.1. X-ray Emission from Galaxy F

Enhanced X-ray emission has been seen in the large elliptical galaxies in the Coma cluster (Vikhlinin et al. 2001). We compared the enhanced emission of galaxy F with the results from Coma. First, we determined the radial profile of the enhancement to determine its size and the appropriate source region for galaxy F. The emission was clearly more extended than the *Chandra* point spread function. We found that the enhancement measured  $\approx 1''.5$ – $2''$  in radius, or roughly 3 kpc at the distance of Abell 13. Vikhlinin et al. (2001) found that the compact cores associated with the brightest galaxies in the Coma cluster had a physical size of 3 kpc in radius.

We attempted to extract a spectrum of the enhanced emission associated with galaxy F from a circular region with radius of  $2''$ . To account for both the cosmic X-ray background and the cluster emission, we used a local background extracted from an annulus centered on galaxy F with radii of  $3''$  and  $5''$ . There are only 31 counts in a  $2''$  region around galaxy F, and we expect 17.5 of these to be background. This is too few counts for spectral fitting or even to determine a useful color for the source. Even a basic color comparison cannot yield any constraint on the temperature of the galaxy gas.

We used PIMMS to determine the flux from galaxy F. We measured a 0.5–8.0 keV count rate of  $2.1 \times 10^{-4}$  cts  $s^{-1}$  and assumed a gas temperature of 1 keV for a Raymond-Smith plasma model. The largest elliptical galaxies have X-ray gas temperatures of  $\approx 1$  keV (e.g., O’Sullivan et al. 2003). From PIMMS we find a 0.5–2.0 keV unabsorbed flux of  $8.2 \times 10^{-16}$  erg  $cm^{-2}$   $s^{-1}$ , or a luminosity of  $2 \times 10^{40}$  erg  $s^{-1}$ . The galaxies in Coma had similar, although slightly larger ( $7.6$ – $9.1 \times 10^{40}$  erg  $s^{-1}$ ) luminosities. We also calculated the mass of gas necessary to produce the excess emission from galaxy F. To do this, we first calculated the model normalization of a 1 keV APEC plasma model that would produce the flux

<sup>13</sup> Available at <http://newwww.ipac.caltech.edu/>

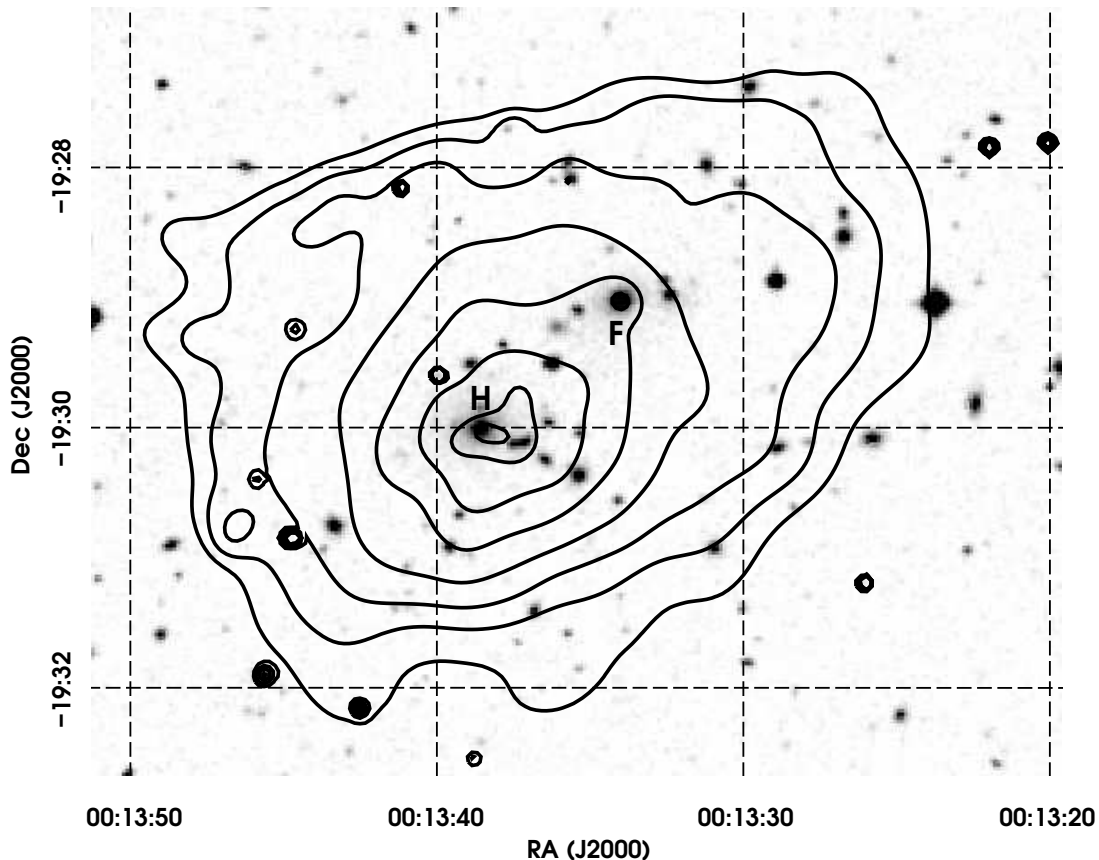


FIG. 2.— X-ray brightness contours (0.3–10 keV band, logarithmically spaced by a factor of  $\sqrt{2}$ ) overlaid on the DSS optical image scanned from a SERC-J survey plate taken in 1977 at the UK Schmidt telescope, Australia. The bright galaxies H and F from Slee et al. (2001) are labeled. The X-ray emission is centered near galaxy H. A knot of X-ray emission to the northwest of the cluster X-ray peak is consistent with the position of galaxy F. The steepness of the X-ray contours on the northern and eastern edges are artifacts of the CCD edge.

measured from galaxy F. We then calculated the average electron number density in the gas from the model normalization and assuming a spherical gas distribution with  $2''$  radius. Translating the electron number density into a gas mass, we find that the required gas mass is  $4.2 \times 10^7 M_{\odot}$ . This is comparable to the gas masses found in the Coma galaxies and other galaxies in nearby clusters (Vikhlinin et al. 2001; Sun et al. 2007).

Given the similarity in size and luminosity, we may expect that the cause of the X-ray enhancement in galaxy F is the same as that found for the Coma galaxies (Vikhlinin et al. 2001). The gas in the Coma galaxies is of low temperature (1–2 keV) and is likely the remains of the galactic X-ray halos. Vikhlinin et al. (2001) suggest that the cool gas is in pressure equilibrium with the hotter, intercluster medium.

### 3. SPECTRAL ANALYSIS

Spectra were extracted from the level 2 event file, excluding point sources within the regions of interest. Background spectra were extracted from the blank-sky background file. For each spectrum, weighted response files (RMFs and ARFs) were generated using the CIAO tools `mkacisrmf` and `mkwarf`, respectively. Finally, spectra were grouped to obtain a minimum of 25 counts per bin. Spectral fitting was primarily performed in XSPEC v11.0, except for the temperature map spectral fits (see § 3.2 below).

#### 3.1. Total Spectrum

We first determined the integrated spectrum of the cluster using an elliptical region with semi-major and semi-minor axes of  $2'.5$  and  $1'.9$ , respectively, and position angle of  $121^{\circ}$  measured from north to east (see Figure 6). This region was the largest elliptical region whose shape agreed with the outer cluster X-ray isophotes and fit entirely on the S3 CCD. We fit the data with an absorbed plasma model, using the APEC model in XSPEC. We fixed the redshift of the cluster to the mean redshift of Abell 13 found in the ENACS study ( $z = 0.0943$ ; Mazure et al. 1996) and the equivalent hydrogen column density to the average Galactic value in the direction of Abell 13,  $N_{\text{H}} = 2.0 \times 10^{20} \text{ cm}^{-2}$  (Dickey & Lockman 1990). The best-fit model had a temperature  $kT = 6.0 \pm 0.3 \text{ keV}$  and a metal abundance of  $0.46 \pm 0.12$  solar (see Table 2 and Figure 7).

We also performed a spectral study to determine if a cooling flow is present in the center of Abell 13, i.e. the peak in the X-ray emission which is also coincident with galaxy H. We extracted spectra in circular annuli out to  $100''$  from the cluster center. Each spectrum was required to have at least 1000 counts. The width of the annuli ranged from  $15''$  in the cluster center to  $5''$  at the periphery of the cluster. We fitted each spectrum with the same APEC model used to describe the total cluster emission, allowing only the temperature and normalization to vary (the metallicity was fixed at the best fit value

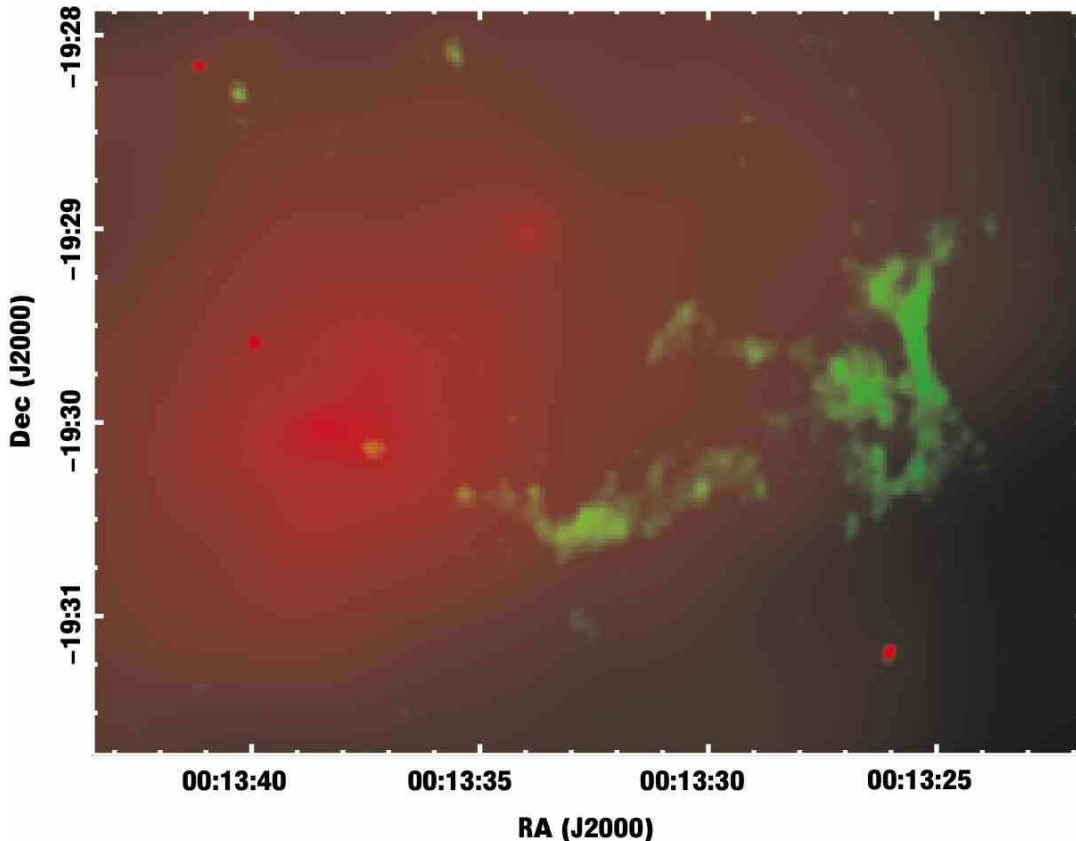


FIG. 3.— Radio image at 1.4 GHz (Slee et al. 2001) overlaid in green the adaptively smoothed X-ray image of Abell 13 in red. North is up, and east is left. The region covered is  $5'.1 \times 3'.8$ . The radio image shows only emission detected at greater than  $2.5\sigma$  as determined by Slee et al. (2001). The three compact red spots are X-ray point sources unrelated to the cluster.

found above). No statistically significant variations in temperature were found. This result is consistent with the temperature map determined in § 3.2.

### 3.2. Temperature Map

In order to determine the spectral distribution in the cluster emission, we created an adaptively binned temperature map of Abell 13, shown in Figure 8. The temperature map was produced using ISIS (Houck & Denicola 2000). A spectrum at each map pixel (1 map pixel =  $16.3$  ACIS pixels =  $8''.0$ ) was extracted from the event data (excluding point sources) in a square region centered on the pixel. The region size was determined by requiring at least 800 net (i.e. background subtracted) counts in the 0.4–7.0 keV energy range, but with a maximum box size of  $183 \times 183$  ACIS pixels, or  $90'' \times 90''$ . The maximum box size was only reached in the outskirts of the cluster. The total counts in each region were between 1.5 and 2 times the 800 count minimum to account for background subtraction. For each spectrum, a background spectrum was extracted from the blank sky background event file in the same region. RMF and ARF files were constructed for specific locations on the CCD, with a spacing of 32 and 50 pixels, respectively. This was done to account for variations in the response across the CCD, without having to create individual RMF and ARF files for each region which would be computationally demanding. For a given region, the RMF and ARF used to fit the spectrum were chosen by selecting the response files with positions clos-

est to the count-weighted average position of the events in each region. The spectra were grouped to have 25 counts per bin and were fitted in ISIS using the APEC thermal model. The Galactic hydrogen column density, redshift, and abundance were fixed to the values found for the full cluster spectrum (§ 3.1 above). Only the temperature and normalization of the APEC model were allowed to vary. In general, the errors on the temperature map are about 20% in the temperature. Although, for pixels with higher best-fit temperatures or those near the edge of the map, the errors are larger, in the range of 50–70%. This is because of the low high-energy sensitivity of *Chandra* and the lower statistics of the outer regions.

The temperature map shown in Figure 8 is colored such that the coolest regions ( $kT \approx 4$  keV) are red, and the hottest regions ( $kT \approx 12$  keV) purple. The intensity contours for the X-ray and radio emission from Abell 13 are overlaid. We note that small differences in temperature from pixel to pixel are not statistically meaningful given the errors in the fits (an average error of 1.2 keV at 6.0 keV). Since the fitted region size is larger than a single map pixel, there is overlap of the fitted regions.

Of particular interest are the lack of very cool gas in the cluster center and the presence of cool gas associated with the radio relic region. The temperature map shows a large concentration of lower temperature gas associated with the radio relic. Below (§3.3) we perform a detailed spectral study of this gas to better constrain its properties. There may also be some hotter gas (purple/blue

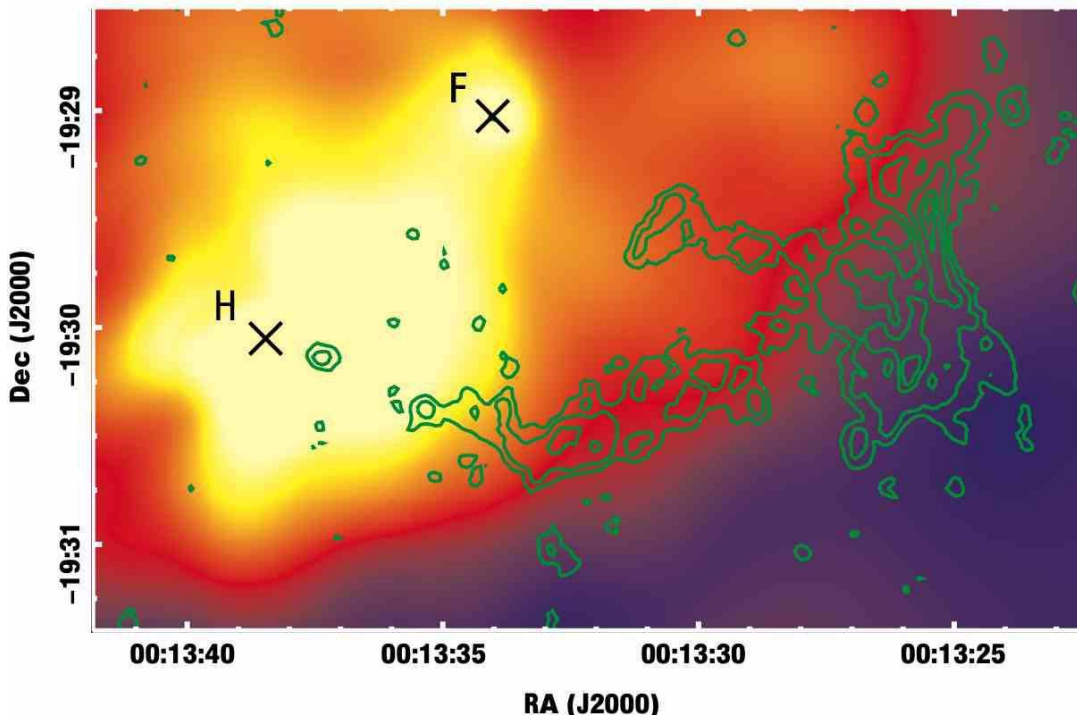


FIG. 4.— Residual X-ray emission from the cluster (color scale from blue=weak to white=strong) after partial subtraction of a smooth elliptical isophotal model for the entire cluster. The region shown here encompasses the radio relic and has a size of  $4'.6 \times 2'.8$ . The color scale was chosen to emphasize the outer regions of the cluster near the radio relic. Overlaid are the radio contours as given in Slee et al. (2001) with contour levels of 43, 86, 173, 303 and  $389 \mu\text{Jy beam}^{-1}$ , which correspond to 2.5, 5, 10, 18 and  $23 \sigma$ . The two brightest galaxies H and F are indicated by the Xs. No excess or clearly associated deficit in X-ray emission is found coincident with the radio relic. Along the eastern tail of the radio emission there appears to be a sharp drop in the residual X-ray emission. However, this drop is not very strong in the total X-ray surface brightness. There is a strong gradient in the southern part of the cluster, but at a larger radius and further south.

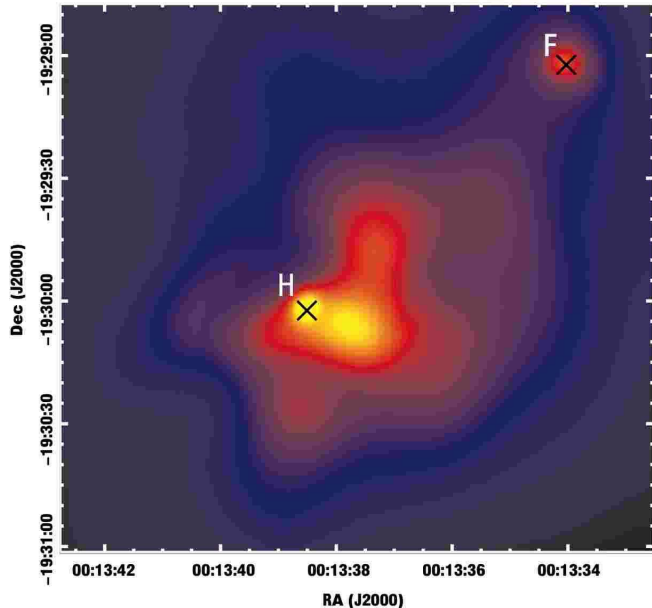


FIG. 5.— Residual emission from center of Abell 13 after partial subtraction of a smooth elliptical isophotal model. The figure spans a region of  $2'.4 \times 2'.2$ . The color scale was chosen to emphasize the inner region of the cluster near galaxy H. North is up and east is left. The bright region marked with an X near the center coincides with galaxy H. Notice the extension of emission to the west (in the direction of the radio relic) and the excess emission perpendicular to that direction. The X at the top right corner marks the position of galaxy F.

region) associated with the steep gradient in the X-ray surface brightness contours on the southern edge of the cluster (see e.g., the X-ray contours in Figure 8) but the temperature errors are large in this region. To try and confirm this result, we extracted spectra on the northern and southern sides of the X-ray gradient. No significant difference in the best-fit temperatures was found, although both regions had large errors. Higher count spectra are required to verify the increased gas temperature along the cluster's southern edge.

### 3.3. X-ray Spectral Study of the Radio Relic Region

From the temperature map, we see that the X-ray emission associated with the radio relic is colder than the average cluster temperature. This immediately rules out a shock origin as we would expect the emission to be hotter in that case. To determine the nature of this cooler emission, we performed a more rigorous X-ray spectral study of the radio relic region. We fit the spectra from a  $2'.0 \times 1'.4$  (major/minor axis) elliptical region surrounding the radio relic (Figure 6). This region was chosen to encompass the outer portion of the radio relic that is associated with the cooler gas in the temperature map. This region has the advantage that it is a region of lower surface brightness for the hot gas component. If we add in the radio relic region to the east (the tail leading back to galaxy H), the spectrum has a much larger hot gas component and is less sensitive to a cool gas component.

The data were fit with different spectral models, including a single temperature gas model, a two-temperature gas model, and a gas + powerlaw emission model. The results are given in Table 3. In all fits we

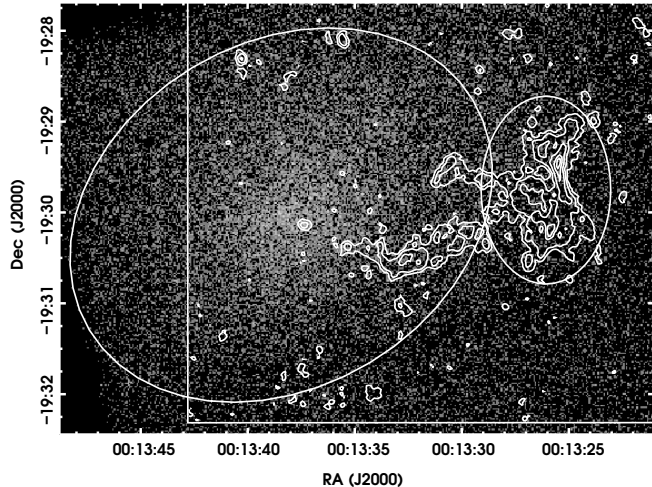


FIG. 6.— Raw *Chandra* X-ray image (0.3–10 keV) of Abell 13 encompassing the cluster center and radio relic positions. Overlaid are the radio contours of Slee et al. (2001). The straight lines mark the coverage of the VLA data compared to the *Chandra* data. The large ellipse marks the region of the data used to determine the spectral model of the full cluster emission (§ 3.1). The smaller ellipse on the right marks the region of the data used to measure the spectrum of the X-ray gas coincident with the radio relic (§ 3.3). The region covered is  $6'6 \times 4'7$ .

TABLE 2  
BEST-FIT APEC MODEL PARAMETERS FOR  
CLUSTER<sup>a</sup>

Parameter	Value
$N_{\text{H}}$ ( $\text{cm}^{-2}$ )	$2.0 \times 10^{20\text{b}}$
$kT$ (keV)	$6.0 \pm 0.3$
Abundance (solar)	$0.46 \pm 0.12$
Norm	$(2.98 \pm 0.08) \times 10^{-3}$
$\chi^2/\text{dof}$	316.45/297

<sup>a</sup> All errors quoted at the 90%-confidence level.

<sup>b</sup> Column density fixed at Galactic value.

have frozen the metallicity of the thermal components to that of the general cluster emission. If allowed to vary, the metallicity is unconstrained. The single temperature gas model, while a decent fit to the data, does not reproduce the excess emission in the data near 0.8 keV (see Figure 9). The two-temperature gas model is the best fit to the data. One of the components is consistent with the overall cluster temperature, while the other component has a temperature of  $\approx 0.9$  keV and accounts for the soft excess seen in the data. The gas + powerlaw model is a worse fit, with the powerlaw component replacing the hotter gas component. The two-temperature gas model is the most appropriate, as it would include both a lower temperature gas associated with the relic as well as hotter cluster emission seen in projection.

#### 4. DISCUSSION

We have presented the *Chandra* data of the galaxy cluster Abell 13. The X-ray emission is centered on galaxy H of Slee et al. (2001), the brightest cluster galaxy. The spatial structure near the core is complicated, with a bright tail of excess emission to the west of galaxy H, and a fainter excess to the north. No point source is associated with galaxy H and no cooling flow is found.

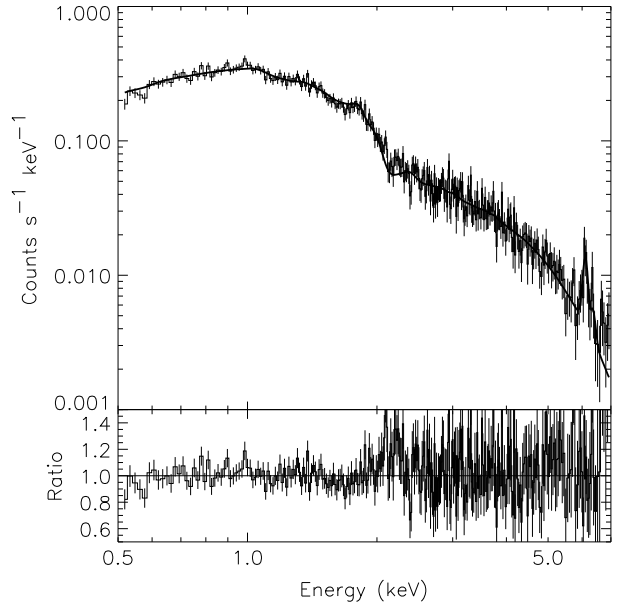


FIG. 7.— *Upper panel*: Count spectrum of the X-ray emission from Abell 13 and the best fit model. *Lower panel*: Ratio of the data and best-fit model (data/model). The spectrum was extracted from a  $2'5 \times 1'9$  elliptical region encompassing the largest elliptical isophote contained fully on the S3 CCD. The best-fit model has a temperature  $kT = 6.0 \pm 0.3$  keV and a metal abundance of 0.46  $\pm$  0.12 solar.

We also found excess X-ray emission associated with the second-brightest elliptical galaxy, F, in the cluster. The mass of gas associated with galaxy F is consistent with other bright elliptical galaxies in cluster environments (Vikhlinin et al. 2001; Sun et al. 2007). In general, there is an extension of the X-ray emission to the northwest with respect to the X-ray peak coincident with galaxy H. Finally, no excess or significant deficit in emission is found coincident with the unusual radio relic in Abell 13, although the spectral properties of the gas in this region are different from those in other areas of the cluster. We found a soft excess in the spectrum of gas coincident with the radio relic, which can be well fit by a  $\approx 0.9$  keV thermal model, suggesting the presence of cooler gas there.

The redshift distribution of the galaxies in Abell 13 can be described by a bimodal distribution (Fadda et al. 1996). The subclumps are not distinguishable in their location on the sky. Interestingly, the two brightest galaxies, H and F, are associated with different peaks in the redshift distribution and rather than being associated with the peak velocity, either of the cluster as a whole or of either subclump, the velocities of galaxies H and F are on the very edges of the velocity distribution. Galaxy F is on the lower edge for the low-velocity subcluster and galaxy H on the higher edge of the high-velocity subcluster. This, combined with the complicated structure of the X-ray emission, points to an ongoing merger within the cluster and that galaxies H and F have a significant velocity relative to the general cluster distribution. The spatial distribution of the galaxies in Abell 13 shows a northwest-southeast extension, paralleling the X-ray distribution, but extending to larger scales.

In the following discussion, we assume that the X-ray gas associated with the radio relic has two components, a hot (6 keV) gas component due to the general cluster

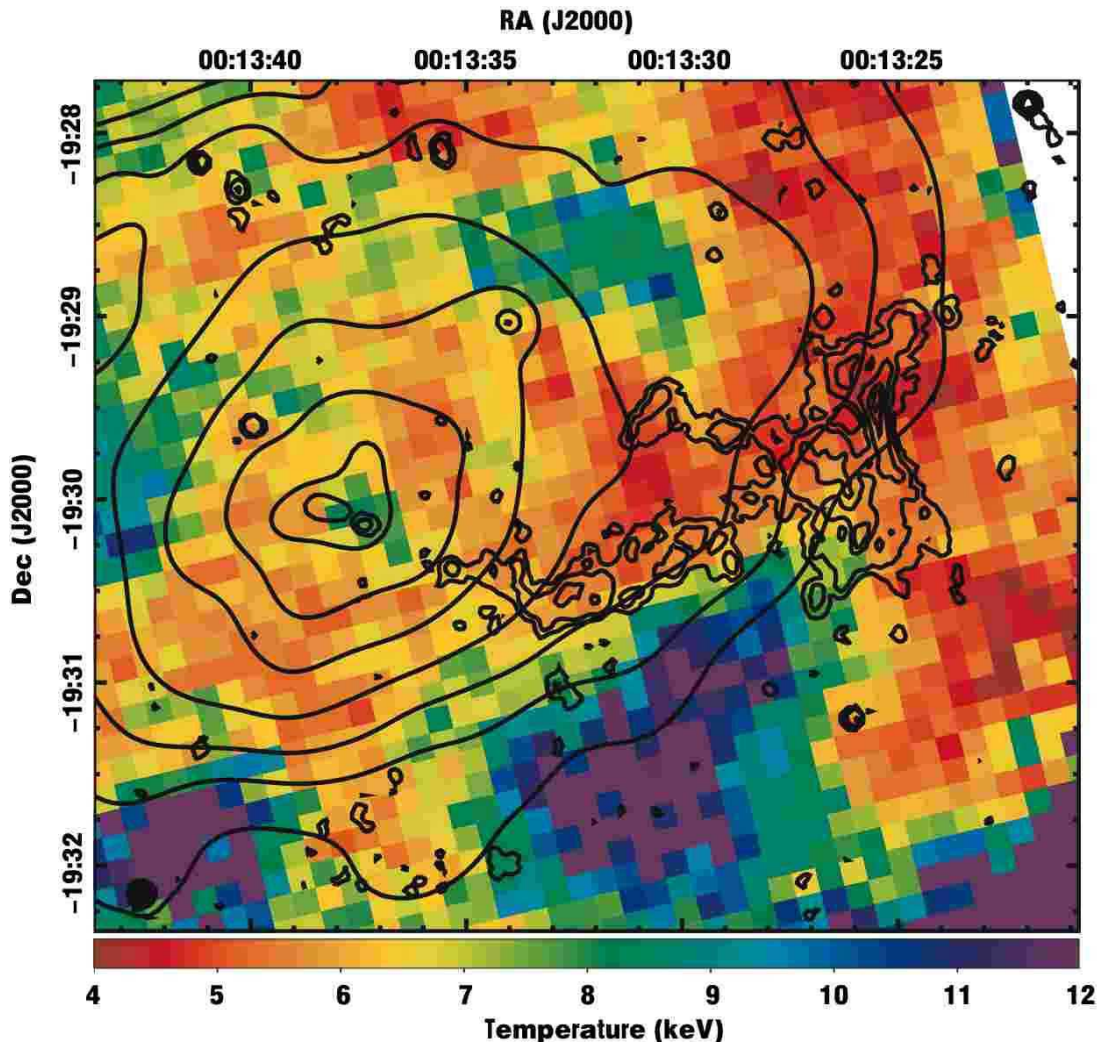


FIG. 8.— Temperature map of Abell 13. Red signifies regions of lower temperature, purple higher temperature. Overlaid are the X-ray and radio surface brightness contours. No cooling flow is detected. The coolest gas is to the west of the peak in the X-ray emission, and apparently associated with the radio relic.

emission, and a cooler (0.9 keV) gas component local to the relic. This model is based on our best-fit spectrum found in § 3.3. We assume that the two components are in pressure equilibrium.

From Slee et al. (2001), the minimum pressure of the radio relic in Abell 13 is  $1.4 \times 10^{-12}$  dyne  $\text{cm}^{-2}$ . Their estimate of the thermal pressure of the hot X-ray gas was very rough and based solely on scaling the properties of Abell 85 since no imaging observation of Abell 13 was available. Our *Chandra* data allow for a more accurate estimate of the thermal pressure at the location of the relic. However, due to an unfortunate placement of the cluster on the CCD, the only regions which extended out to a distance larger than the relic were in the direction of the relic and to the south. Since the southern edge of the cluster shows a steep gradient in the X-ray emission, we did not consider this region in determining the surface brightness distribution. Instead, we determined the surface brightness of the cluster in a conical region extending from the cluster center out to  $4/1$  and encompassing position angles of  $240\text{--}312^\circ$  measured from the north to the east. This region includes the radio relic and associated cool gas which will affect our results; however, while not a perfect measure of the properties of the X-

ray gas, it represents a significant improvement on the estimates of Slee et al. (2001). A larger field of view observation would be better suited to address the surface brightness and electron density distributions of the full cluster emission.

Using the surface brightness distribution, we estimate the electron density distribution of the hot component following the spherical deprojection method of Kriss et al. (1983). We assumed a single temperature of the hot gas of 6.0 keV and used the APEC thermal model to convert from counts to electron density. From this, we find an electron density at the relic of  $1 \times 10^{-3}$   $\text{cm}^{-3}$ . Given this and the average cluster temperature (6.0 keV) determined in § 3.1, we find that the thermal pressure of the surrounding hot gas at the location of the radio relic is  $1.6 \times 10^{-11}$  dyne  $\text{cm}^{-2}$ . This value is larger than the estimate for the pressure of the radio plasma, as has been seen in other X-ray cluster radio bubbles (Dunn et al. 2005). We note that if the relic were at a larger radius than the projected radius, the electron density and thermal pressure would be lower, bringing it closer to the radio plasma pressure estimate. In addition, in the case of Abell 13, if the values assumed by Slee et al. (2001) for (1) the ratio of masses in heavy particles and electrons;



TABLE 3  
BEST-FIT X-RAY SPECTRAL MODEL PARAMETERS FOR RADIO RELIC<sup>a</sup>

Model	$kT_1$ (keV)	Norm <sub>1</sub>	$kT_2$ or $\Gamma$	Norm <sub>2</sub>	$\chi^2/\text{dof}$
APEC	$5.9^{+1.9}_{-1.1}$	$(1.77 \pm 0.08) \times 10^{-4}$	...	...	89.4/69
APEC + APEC	$0.86^{+0.16}_{-0.09}$	$(1.5 \pm 0.8) \times 10^{-5}$	$10^{+12}_{-4}$	$(1.60 \pm 0.12) \times 10^{-4}$	74.3/67
APEC + PL	$0.89^{+0.16}_{-0.09}$	$(1.8 \pm 0.8) \times 10^{-5}$	$1.40 \pm 0.08$	$(3.2 \pm 0.3) \times 10^{-5}$	81.4/67

<sup>a</sup> All errors quoted at the 90%-confidence level. All models were fit including Galactic absorption of  $2.0 \times 10^{20} \text{ cm}^{-2}$ . Abundances for gas emission models were fixed to the best-fit value from the cluster spectrum, 0.46 of solar. The model parameters Norm<sub>1</sub> and Norm<sub>2</sub> are the values of the first and second model component normalizations.  $kT_2$  or  $\Gamma$  is the value of the second model component temperature if APEC or photon index if powerlaw.

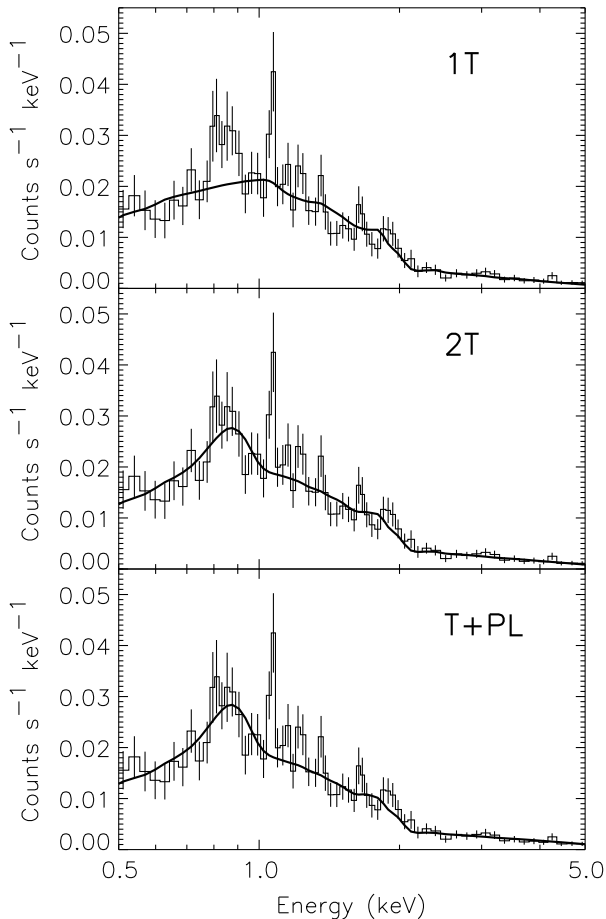


FIG. 9.— Count spectra of the X-ray emission associated with the radio relic, fit with different models. We have fit the spectrum with a single temperature APEC model (*top panel*), two APEC models (*middle panel*), and a powerlaw + APEC model (*bottom panel*). Notice the soft excess at 0.8 keV in the single temperature model (*top*) but not the other spectra. The peak at  $\sim 1.1$  keV is too narrow to be astrophysical and is likely strengthened by binning. At other binnings, it is not as significant.

(2) the plasma filling factor; (3) the low frequency spectral index, and (4) the angle between the line of sight and field direction are given more realistic values then we may increase the radio plasma pressure to that of the confining X-ray gas.

#### 4.1. Origin of the Radio Relic

It is unlikely that the radio relic in Abell 13 is a peripheral cluster relic associated with a cluster merger shock.

First, there is no evidence in the *Chandra* image or spectra for any shock feature near the relic. Second, the radio image shows a long filament which extends almost all the way back to the brightest elliptical galaxy H (Figure 3). Thus, we assume that the radio emitting plasma originated in an AGN at the center of galaxy H. Based on the classification system of Kempner et al. (2004), which looks at the physical properties and proposed origins of extended cluster radio sources, we would classify Abell 13 as an AGN relic system.

We propose two explanations for the multi-wavelength properties of Abell 13. The first is the buoyant bubble scenario suggested by Fujita et al. (2002) for Abell 133. The radio source may have uplifted the cool gas from the core of Abell 13. In this scenario, galaxy H would have been an active radio emitter in the past. At some later time, the radio plasma would have risen by buoyancy, and entrained the cool gas in the center, uplifting it to a larger distance from the cluster center. This might also remove the source of fuel for the central AGN. This would explain the lack of cool gas in the cluster center and the fact that currently, galaxy H is neither a radio ( $< 0.1$  mJy at 1.4 GHz; Slee et al. 2001) nor a hard X-ray source. To estimate the time scale for the cool gas and radio source to rise by buoyancy from the position of galaxy H, we assume that the cool gas and radio source move at a velocity roughly 1/3 the sound speed,  $c_s$ , of the hot gas component. For a 6.0 keV gas,  $c_s$  is 980 km s<sup>-1</sup>. The projected separation between the relic and galaxy H is 2'2"-3'1". This yields a buoyancy time scale of  $7\text{--}10 \times 10^8$  yr, roughly consistent with the relic age determined through spectral fitting (Slee et al. 2001). To estimate the mass of cool gas uplifted, we take the volume to be that of a prolate spheroid with major and minor axes equal to that of the region used to extract the spectrum of the radio relic. From the two-temperature spectral model, we find that the enclosed mass of cool gas is  $\sim 2 \times 10^{10} M_\odot$ . This is a factor of 10 greater than the mass of gas contained in the tongue of X-ray gas found in Abell 133 (Fujita et al. 2002). However, we note that the electron density for the cool gas is  $\sim 5 \times 10^{-4} \text{ cm}^{-3}$ , lower than the hotter cluster gas (particularly the gas towards the center of the cluster) making buoyant uplift a possibility. A cool gas mass of  $\sim 2 \times 10^{10} M_\odot$  implies that previously Abell 13 would have had a mass deposition rate of  $\sim 2 M_\odot \text{ yr}^{-1}$  assuming a cooling time of  $10^{10}$  yr. This is on the low end of the distribution of known cooling flow mass deposition rates (see e.g., White et al. 1997). This is only an estimate of the mass of cool gas to determine if the value

is realistic. The temperature map shows additional cool regions to the north and east of the radio relic which if taken into account would increase the mass of cool gas. However, the radio relic is filamentary in structure and it is possible that the cool gas also resides in filaments rather than a single big blob, which would decrease the gas mass estimate. Since it is difficult to determine the extent of either of these situations, we merely suggest that the estimated amount of cool gas in Abell 13 seems reasonable for a galaxy cluster.

The lower temperature of the gas near the radio source might be due both to the lower entropy of the gas in the cool core of the cluster, plus the effects of adiabatic expansion as this gas was moved out to a lower-pressure region. From our above estimate of the electron density distribution of the cluster gas, we find that the electron density at the cluster center is  $\approx 6$  times that at the radio relic. The pressure difference between the two locations should also be 6 times assuming a constant hot gas temperature. We assume that the cool gas component is always in pressure equilibrium with the hot gas component that dominates the cluster emission. As a result of adiabatic expansion, the temperature of the cool gas in its current location,  $T_2$  is related to its initial temperature,  $T_1$ , by

$$T_2 = T_1 \left( \frac{P_2}{P_1} \right)^{(\gamma-1)/\gamma} = T_1 \left( \frac{P_2}{P_1} \right)^{2/5}, \quad (1)$$

where  $P_1$  is the pressure in the cluster core and  $P_2$  is the pressure at the location of the radio relic, and the adiabatic index is  $\gamma = 5/3$ . Observationally, we found  $P_1/P_2 \approx 6$ , giving  $T_2 \approx 0.5 T_1$  for adiabatic expansion. This difference alone cannot account for the cooling of the gas from the average cluster temperature of  $\approx 6$  keV to its current temperature of  $\approx 0.9$  keV. Therefore, the cool gas associated with the radio relic must have been cooler than the average cluster temperature to begin with. We can estimate the initial cool gas temperature assuming that adiabatic expansion was the only heating or cooling mechanism as the cool gas was uplifted. This requires that the initial temperature of the cool gas was about  $T_1 \approx 2$  keV when this gas was located at the cluster core. This is a reasonable temperature for a cooling core. If the relic were at a larger radius than the projected radius, then we would expect the electron density to be lower and therefore the adiabatic cooling to be stronger. This would make the initial temperature of the cool gas higher, possibly more in line with the average

cluster temperature.

Our second proposed explanation is that a dynamical event is the origin of the unusual radio relic and disturbed X-ray morphology. Both the X-ray and optical properties (radial velocity distribution) suggest that Abell 13 is undergoing a merger event. The X-ray extension from galaxy H (to the west) points back to the radio relic. This may imply that galaxy H is moving to the east and that the radio relic is at the former position of the galaxy. (We note that the extension may also favor the buoyant uplift scenario.) We propose that before the merger event, galaxy H had a cool core and showed AGN activity. As the merger progressed, the cold core and radio lobes were displaced (or stripped) from the galaxy as a result of ram pressure from the gas in the other subcluster, which did not affect the stars and dark matter in galaxy H. Slee et al. (2001) found that the travel time from galaxy H was comparable to the estimated relic age. The long filament of radio emission leading back almost to galaxy H (Figure 3) suggests that the AGN remained active during the initial phases of this stripping process. The concentration of X-ray emission around galaxy H (Figure 5) suggests that the stripping process is not complete; there is still gas around galaxy H, but it is relatively hot, perhaps due to heating processes associated with the merger. The *Chandra* data do not conclusively determine which of these two models is correct, or strongly reject either.

We would like to thank Gregory Sivakoff and Marios Chatzikos for useful discussions. We would also like to thank the anonymous referee whose comments helped to improve the paper. Support for this work was provided by the National Aeronautics and Space Administration primarily through *Chandra* award GO4-5133X, but also through GO4-5137X and GO5-6126X, issued by the Chandra X-ray Observatory, which is operated by the Smithsonian Astrophysical Observatory for and on behalf of NASA under contract NAS8-39073. Some support also came from NASA XMM-Newton award NNG04GO34G. Basic research in radio astronomy at NRL is supported by 6.1 Base funding. HA acknowledges support from CONACyT grant 40094-F. Y. F. is supported in part by a Grant-in-Aid from the Ministry of Education, Culture, Sports, Science, and Technology of Japan (17740162). L. R. acknowledges support from the National Science Foundation under grants AST-0307600 and AST-0607674 to the University of Minnesota.

#### REFERENCES

- Böhringer, H., Voges, W., Fabian, A. C., Edge, A. C., & Neumann, D. M. 1993, MNRAS, 264, L25  
 Brandt, W. N., et al. 2001, AJ, 122, 2810  
 Dickey, J. M., & Lockman, F. J. 1990, ARA&A, 28, 215  
 Dunn, R. J. H., Fabian, A. C. & Taylor, G. B. 2005, MNRAS, 364, 1343  
 Fabian, A. C., et al. 2000, MNRAS, 318, L65  
 Fadda, D., Girardi, M., Giuricin, G., Mardirossian, F., & Mezzetti, M. 1996, ApJ, 473, 670  
 Fujita, Y., Sarazin, C. L., Kempner, J. C., Rudnick, L., Slee, O. B., Roy, A. L., Andernach, H., & Ehle, M. 2002, ApJ, 575, 764  
 Fujita, Y., Sarazin, C. L., Reiprich, T. H., Andernach, H., Ehle, M., Murgia, M., Rudnick, L., & Slee, O. B. 2004, ApJ, 616, 157  
 Garmire, G. P., Bautz, M. W., Ford, P. G., Nousek, J. A., & Ricker, G. R. 2003, Proc. SPIE, 4851, 28  
 Giacconi, R., et al. 2001, ApJ, 551, 624  
 Giovannini, G., & Feretti, L. 2004, J. Korean Astron. Soc., 37, 323  
 Giovannini, G., Feretti, L., & Stanghellini, C. 1991, A&A, 252, 528  
 Houck, J. C., & Denicola, L. A. 2000, in ASP Conf. Ser. 216: Astronomical Data Analysis Software and Systems IX, ed. N. Manset, C. Veillet, & D. Crabtree (San Francisco: ASP), 591  
 Kempner, J. C., Blanton, E. L., Clarke, T. E., Enßlin, T. A., Johnston-Hollitt, M., & Rudnick, L. 2004, in The Riddle of Cooling Flows in Galaxies and Clusters of galaxies, ed. T. Reiprich, J. Kempner, & N. Soker (Charlottesville: Univ. Virginia), 335  
 Kriss, G. A., Cioffi, D. F., & Canizares, C. R. 1983, ApJ, 272, 439  
 Mazure, A., et al. 1996, A&A, 310, 31  
 O'Sullivan, E., Ponman, T. J., & Collins, R. S. 2003, MNRAS, 340, 1375  
 Quintana, H., & Ramírez, A. 1995, ApJS, 96, 343

- Röttgering, H. J. A., Wieringa, M. H., Hunstead, R. W., & Ekers, R. D. 1997, *MNRAS*, 290, 577
- Slee, O. B., Roy, A. L., Murgia, M., Andernach, H., & Ehle, M. 2001, *AJ*, 122, 1172
- Sun, M., Jones, C., Forman, W., Vikhlinin, A., Donahue, M., & Voit, M. 2007, *ApJ*, 657, 197
- Vikhlinin, A., Markevitch, M., Forman, W., & Jones, C. 2001, *ApJ*, 555, L87
- White, D. A., Jones, C., & Forman, W. 1997, *MNRAS*, 292, 419